IEEE Photonics Journal
An IEEE Photonics Society Publication

Open Access

DFB Semiconductor Laser With Discrete Coupling Coefficient Based on the Equivalent Technique

Volume 7, Number 3, June 2015

Junshou Zheng
Duotian Xia
Song Tang
Yuechun Shi
Jilin Zheng
Jun Lu
Xiangfei Chen
Yunshan Zhang

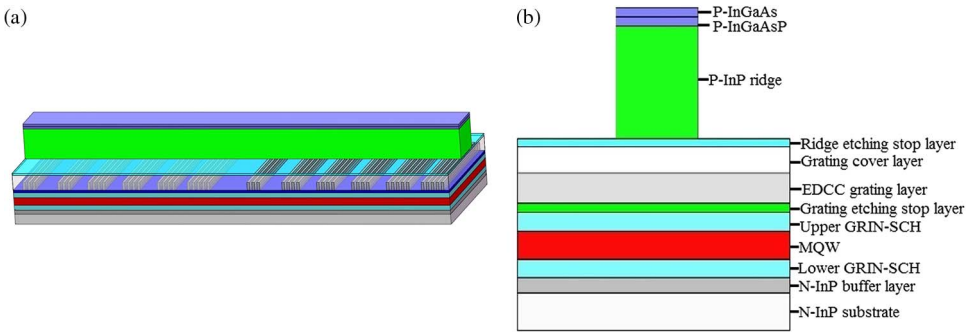

DOI: 10.1109/JPHOT.2015.2426872
1943-0655

IEEE photonics SOCIETY

IEEE

DFB Semiconductor Laser With Discrete Coupling Coefficient Based on the Equivalent Technique

Junshou Zheng,[1] Duotian Xia,[1] Song Tang,[1] Yuechun Shi,[1] Jilin Zheng,[1,3] Jun Lu,[1] Xiangfei Chen,[1,2] and Yunshan Zhang[1,2]

[1]College of Engineering and Applied Sciences, Nanjing University, Nanjing 210093, China
[2]Nanjing University (Suzhou) High-Tech Institute, Suzhou 215123, China
[3]Institute of Communication Engineering, PLA University of Science and Technology, Nanjing 210007, China

DOI: 10.1109/JPHOT.2015.2426872

Manuscript received January 13, 2015; revised April 13, 2015; accepted April 21, 2015. Date of publication April 29, 2015; date of current version May 27, 2015. This work was supported in part by the National Natural Science Foundation of China under Grant 61090392 and Grant 61435014; by the Fundamental Research Funds for the Central Universities and PAPD, Jiangsu Province, China; by the National Natural Science Foundation for the Youth under Grant 61306068; by the Natural Science Foundation of Jiangsu Province of Youth under Grant BK2012058, Grant BK20130585, and Grant BK20140414; and by the Technology Support Program of Jiangsu Province under Grant BE2012157.
Corresponding author: Y. Zhang (e-mail: zys5014@163.com).

Abstract: An equivalently discrete coupling coefficient (EDCC) distributed feedback (DFB) semiconductor laser with EDCC grating is numerically investigated and experimentally demonstrated; the EDCC grating structure is designed by discretizing the duty cycle of sampled Bragg grating along the laser cavity, i.e., the cavity is divided into some subsections, and the duty cycle is constant in each subsection while it is different between two adjacent subsections, instead of the truly discrete coupling coefficient grating profile realized by discontinuously varying the duty cycle and/or etching depth of the uniform gating pitch. Moreover, the EDCC grating is fabricated by combining the conventional holographic exposure with a micrometer-level photolithography, which will simplify the fabrication process and reduce the fabrication cost. Based on experimental data, the analysis of spectral behavior as a function of injection current shows that the stable single-longitudinal-mode operation has been realized, even at large injection current and high temperature.

Index Terms: Discrete coupling coefficient, semiconductor lasers, distributed feedback (DFB), single-longitudinal-mode operation.

1. Introduction

Distributed feedback (DFB) semiconductor lasers are widely used as light sources in the optical communication systems. Stable single-longitudinal-mode (SLM) operation with high side mode suppression ratio (SMSR) is very important for practical applications. To obtain stable SLM operation, many special structures have been proposed, such as the multiple phase shifts (MPS) [1], multiple electrode (MEL) structure [2], and corrugation-pitch modulated (CPM) structure [3]. Moreover, it also has been reported that distributed coupling coefficient DFB laser with stronger coupling coefficient in the center has stable single longitudinal mode operation, because the

side-lobe in the reflection spectrum of the passive gratings is effectively suppressed [4]. However, the injection current is limited to a narrow range since the SMSR deteriorates as the injection current increases to a higher level. The analysis results indicate that the stronger center coupling and weaker side coupling structure can intensify the longitudinal spatial hole burning (LSHB) under high injection current level. Therefore, in order to realize the stable SLM operation, scientific researchers are still investigating new techniques [5]–[7].

Recently, the Reconstruction-Equivalent-Chirp (REC) technique based on the Sampled Bragg grating (SBG) has been successfully applied to design and fabricate DFB semiconductor lasers [8]–[10] and laser arrays [11]–[14]. Based on the REC technique, the various grating structures can be equivalently realized by only changing the sampling parameters while the seed grating is kept uniform.

In this paper, we propose a novel DFB semiconductor laser with equivalently discrete coupling coefficient (EDCC) to realize the stable SLM operation. This discrete coupling coefficient (DCC) DFB semiconductor laser is difficult to obtain by the conventional method, because it is hard to realize the truly discrete variation in the duty cycle and/or the etching depth of the uniform grating pitch along the laser cavity. However, based on the REC technique, the EDCC grating profile can be realized by discretely changing the duty cycle of the SBG along the laser cavity.

2. Principle and Design

Based on the Fourier analysis, if the sampling period remains unchanged, but a pitch error ΔP is introduced at position z_0, the index modulation of the mth order subgrating can be expressed as [8], [12], [15]

$$\Delta n_m(z) = \begin{cases} \frac{1}{2} F_m \Delta n_s \exp\left(j\frac{2\pi z}{\Lambda_m}\right) + \text{c.c}, & z \le z_0 \\ \frac{1}{2} F_m \Delta n_s \exp\left(j\frac{2\pi z}{\Lambda_m}\right) \exp\left(-j\frac{2m\pi\Delta P}{P}\right) + \text{c.c}, & z > z_0 \end{cases} \tag{1}$$

where F_m is the Fourier coefficient, m denotes the order Fourier series, Δn_s is the index modulation of the uniform seed grating, and z is the position along the laser cavity. Λ_m is the grating period of the mth order subgrating, which can be expressed as

$$\Lambda_m = \frac{\Lambda_0 P}{m\Lambda_0 + P} \tag{2}$$

where P is the sampling period, and Λ_0 is the period of the uniform seed grating. According to (1), an equivalent phase shift (EPS) $\theta = -2m\pi\Delta P/P$ can be obtained in each mth order subgrating.

Usually, the $+1$st/-1st order subgrating is used as the working channel in the DFB semiconductor laser based on the REC technique [8]–[12], [15]. For simplicity, the amplitude of the Fourier coefficient $F_{\pm 1}$ is investigated here only, which can be expressed as

$$|F_{\pm 1}| = \frac{\sin(\pi\gamma)}{\pi} \tag{3}$$

where γ is the duty cycle of the sampling function [9], [16]. $F_{\pm 1}$ is used to measure the index modulation of the ± 1st subgrating.

As shown in Fig. 1, when $\gamma = 0.5$, the $|F_{\pm 1}|$ has the largest value, i.e., 0.5 is the optimum duty cycle of a SBG. Additionally, $|F_{\pm 1}|$ are symmetric about the duty cycle of 0.5. More importantly, the various variations in the index modulation of the ± 1st order subgrating can be equivalently realized only by accordingly changing the duty cycle of the SBG.

The EDCC grating profile is plotted in Fig. 2. An equivalent π phase shift (π-EPS) is introduced into the middle of the laser cavity. The coupling coefficient is discretely distributed along the laser cavity, and the cavity is divided into six subsections, the length of each subsection is much longer than a sampling period. The length of the six subsections is symmetric about the

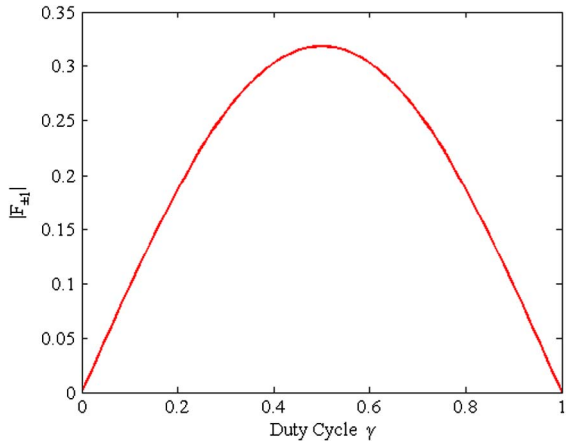

Fig. 1. Relation between $|F_{\pm 1}|$ and the duty cycle.

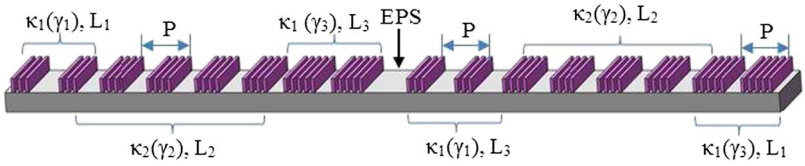

Fig. 2. Schematic diagrams of the EDCC grating structure.

EPS. The duty cycle is discretized to realize the above design, i.e., the duty cycle is constant in each subsection and different between the two adjacent subsections while all the sampling periods are the same. Moreover, the γ_2 is the optimum duty cycle 0.5, γ_1 is smaller or larger than γ_2, the sum of γ_1 and γ_3 is 1.0, and therefore, based on Eq. (3) and Fig. 1, the κ_1 is equal to κ_3 and smaller than κ_2. The specific length of the each subsection is determined after optimizing.

3. Simulation Analysis

The transmission spectrum of the EDCC grating with π-EPS is simulated and plotted as the red line in Fig. 3(a). As a comparison, the equivalently uniform coupling coefficient (EUCC) grating (i.e., all of the duty cycles are 0.5) is also simulated and plotted as the black line in Fig. 3(a), to demonstrate the basic principle of the π-EPS. The black line shows that there is a transmission peak in the center of the stop band of the $+1$st channel, locating at the Bragg wavelength. That is to say, the π phase-shift is equivalently introduced into the $+1$st channel, but there is no transmission peak in the stop band of the 0th order. Moreover, the EDCC grating has the same transmission spectrum compared with the EUCC grating, and the two transmission peaks are overlapped, so the desired wavelength in the $+1$st subgrating of the EDCC grating is the same as the EUCC grating. It can be seen from the insets in Fig. 3(a) that the equivalent apodization is introduced only into the $+1$st subgrating and the side-lobes are greatly decreased. The corresponding group delays are plotted in Fig. 3(b). The group delay indicates the interactive time between the light and the grating structure; therefore, a small group delay means a small total gain during the interaction. From the insets in Fig. 3(b), compared with the EUCC grating, the group delay of the side modes in the EDCC grating are effectively suppressed, which is consistent with the transmission spectrum. The light intensity distributions of the EDCC and EUCC laser are simulated and plotted in Fig. 4, compared with the EUCC DFB laser structure, the central peak intensity is decreased, the LSHB can be effectively reduced in our designed EDCC DFB laser.

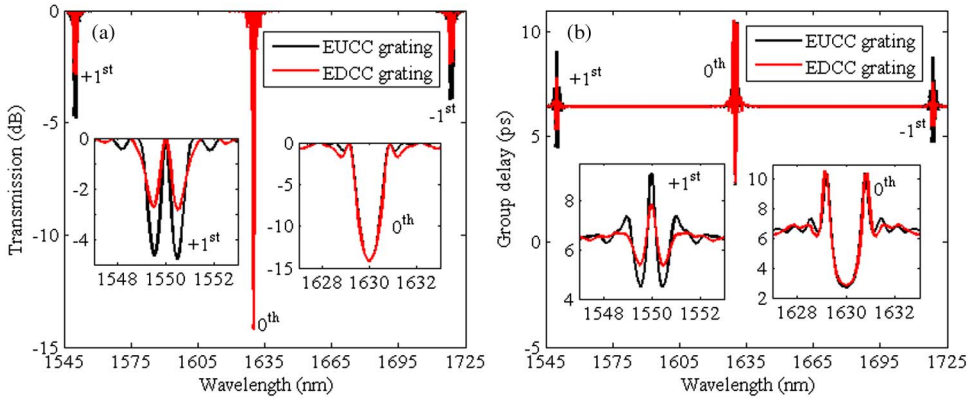

Fig. 3. (a) Transmission spectrums of the EUCC grating and EDCC grating with EPS. (b) Corresponding group delay. (Insets) Close-up views of the +1st and 0th channel.

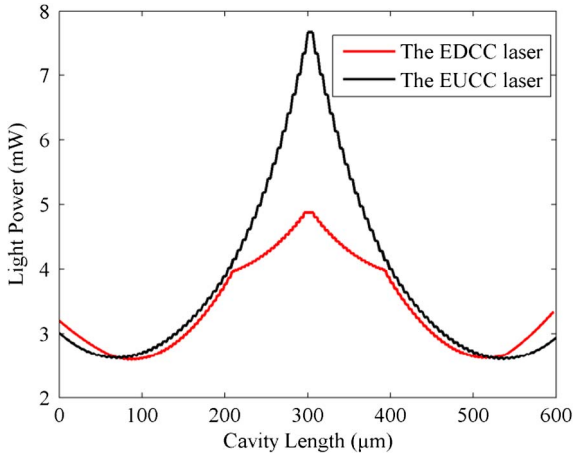

Fig. 4. Light intensity distributions of the EDCC and EUCC DFB laser.

4. Fabrication and Experimental Results

The proposed EDCC DFB laser is fabricated by a conventional two-stage lower-pressure metal-organic vapor phase epitaxy (MOVPE). An InP buffer layer, a graded $In_{1-x-y}Al_xGa_yAs$ lower separate confinement heterostructure (SCH), a multiple quantum-well (MQW) active structure and a graded $In_{1-x-y}Al_xGa_yAs$ upper SCH, an InP etching stop layer and a 1.42Q InGaAsP grating layer are successively grown on an n-InP (100) substrate in the first epitaxial growth. The MQW structure contains five undoped 6 nm-thick +1.2% compressive strain $In_{1-x-y}Al_xGa_yAs$ quantum wells separated by six undoped 9 nm-thick −0.45% tensile strain $In_{1-x-y}Al_xGa_yAs$ barriers. The EDCC grating is formed by combining the conventional holographic lithography with photolithography. In our experiment, the cavity length is 600 μm, the period of the seed gating is 256.29 nm and the Bragg wavelength of 0th channel is about 1630 nm. The sampling period is 5.74 μm. $\gamma_1 = 0.25$, $\gamma_2 = 0.5$, and $\gamma_3 = 0.75$, and in the meantime, $L_1 = 90$ μm, $L_2 = 150$ μm, and $L_3 = 60$ μm. Anti-reflection (AR) is coated on the both facets of the each laser to avoid the influence of the random facet phase. A schematic illustration of the EDCC DFB laser is shown in Fig. 5.

Fig. 6 shows the power–current (P–I) curves of the EDCC laser at the temperature of 25 °C, 35 °C, 45 °C, and 55 °C, respectively. The threshold current is about 32 mA and the slope efficiency is 0.17 mW/mA at the temperature of 25 °C. The threshold current is relatively high and the slope efficiency is relative low because [15], [16], compared with a shorter cavity laser, the

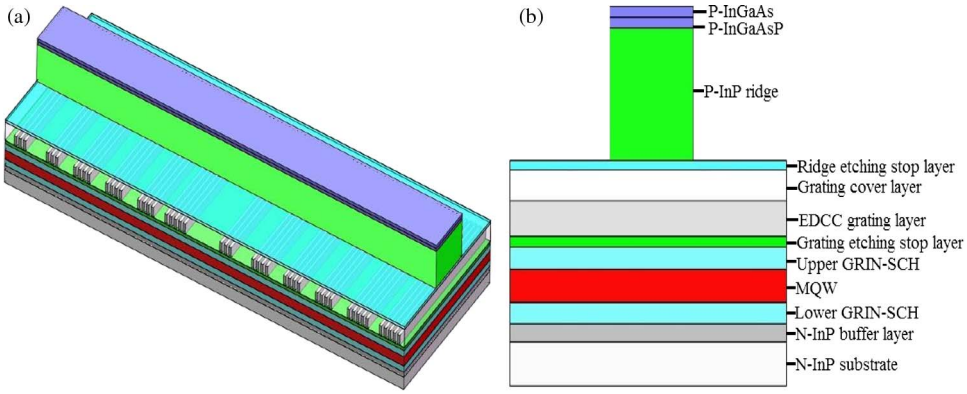

Fig. 5. (a) Schematic diagram of EDCC DFB ridge waveguide laser. (b) Cross sectional view at facet (GRIN-SCH: grade index separate confinement heterostructure).

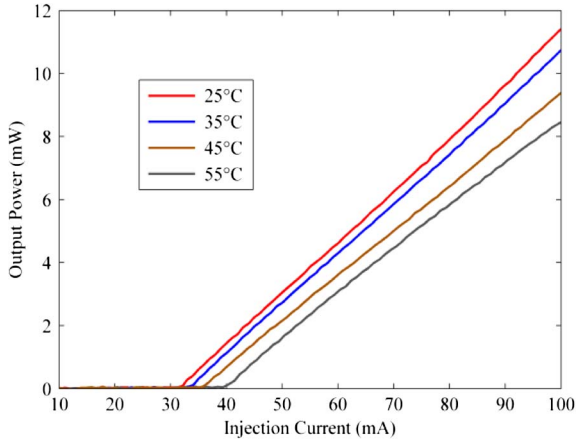

Fig. 6. Measured P–I curves at different surrounding temperatures.

longer cavity laser has a larger injection area in the active region, therefore, the long cavity laser has a higher threshold current to satisfy the threshold condition, and the ratio between the output power and the bias current is smaller. Consequentially, the slope efficiency of a long cavity laser is also lower than that of a short cavity laser. Furthermore, the AR/AR coating is used to avoid the random facet phase and to improve the stability of the lasing mode, but at the moment, the output power at both facets is symmetric. Therefore, the output efficiency is significantly reduced from one facet. The AR/AR coating is tradeoff between the stability of SLM operation and the high slope efficiency. However, the above issues will be improved by using the buried heterostructure waveguide structure [17], and/or increasing the etching depth of the seed grating pitch.

In order to confirm, the side-lobes are effectively suppressed according to the analysis of the transmission spectrum and group delay, and stable single longitudinal mode operation is realized in the EDCC DFB laser. The spectrums of the EDCC DFB laser were measured with the injection current changed from 40 to 160 mA under the temperature of 25 °C, as shown in Fig. 7(a). As for the spectrums, a resonant peak appears closely at the center of the stopband even at the low injection current of 40 mA. The main mode is selectively enhanced as the injection current increases, and a stable SLM operation is realized up to the injection current increased to 160 mA. The side mode suppression ratios (SMSRs) of the left and right side mode in the spectrums as a function of the injection current are plotted in Fig. 7(b). It can be seen that the SMSRs of the left and right side modes increase with the injection current, respectively, and the SMSR of the left side mode $(\mathrm{SMSR_L})$ is slightly larger than the SMSR of the right side mode $(\mathrm{SMSR_R})$ under

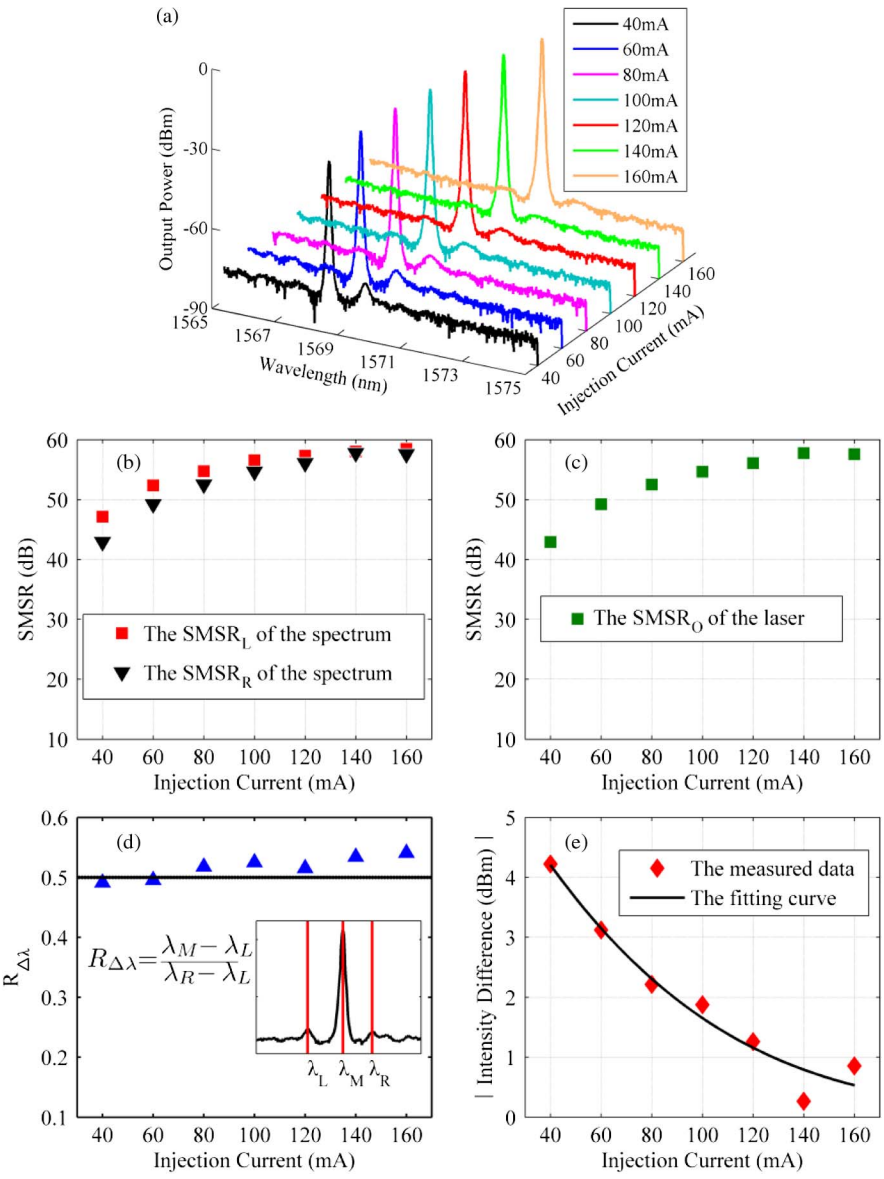

Fig. 7. (a) Measured spectrums of the laser operated under the injection current range from 40 to 160 mA; (b) corresponding SMSRs of the left and right side mode, respectively; (c) the corresponding output SMSRs; (d) dependence of the deviation of the main mode from the center of the stopband on the injection current; and (e) corresponding intensity difference between the left and right side mode.

the low injection level, the reason is that a small peak due to TM mode is observed under the relatively low injection current [18], [19], but it is gradually suppressed with the injection increasing, therefore, the SMSRs of the two side modes tend to be equal as the injection current increasing, as shown in Fig. 7(b). The output SMSR $(\mathrm{SMSR_O})$ of the laser is the smallest value of the $\mathrm{SMSR_L}$ and $\mathrm{SMSR_L}$, which is plotted in Fig. 7(c). It is can be seen that the EDCC laser always operate with high SMSR even at high injection current.

To confirm that the LSHB effect is effectively reduced in the EDCC DFB laser, the dependence of the wavelengths of the main mode and the two side modes on the injection current is analyzed in detail based on the measured data. The deviation from the center of the stopband is evaluated by the parameter $R_{\Delta\lambda} = (\lambda_\mathrm{M} - \lambda_\mathrm{L})/(\lambda_\mathrm{R} - \lambda_\mathrm{L})$, where λ_M is the corresponding

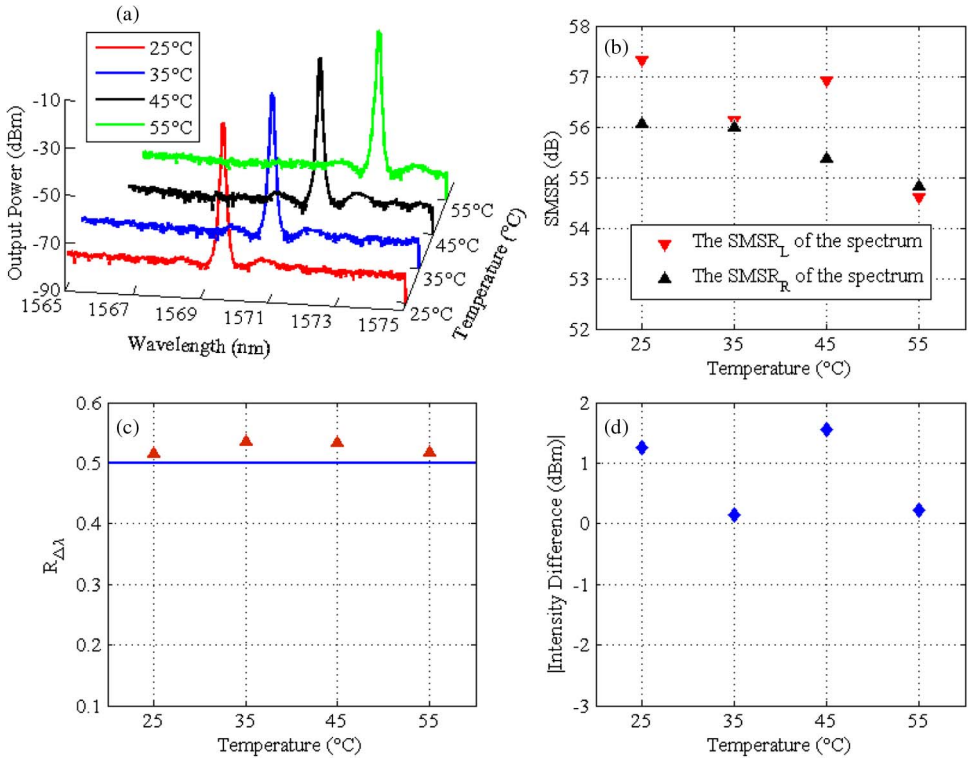

Fig. 8. Characteristics of the laser at the same injection current of 120 mA with the temperature is 25 °C, 35 °C, 45 °C, and 55 °C, respectively. (a) Measured lasing spectrums, (b) corresponding SMSRs of the left and right side modes, (c) dependence of the deviation of the main mode from the center of the stopband on the temperature, and (d) corresponding intensity difference between the left and right side mode.

wavelength of the main mode, λ_L corresponds to the left side mode, and λ_R corresponds to the right mode. Needless to say, $R_{\Delta\lambda} = 0.5$ indicates the main mode locates at the center. The analytical results on the wavelength stability of the EDCC DFB laser are plotted in Fig. 7(d). It is found that the $R_{\Delta\lambda}$ is a little less than 0.5 when the injection current is relatively low, i.e., the main mode slightly deviate from the center of the stopband to the left side mode. Meanwhile, slight asymmetry in the intensities of the left and right side modes, can be observed when the injection current are 40 and 60 mA in Fig. 7(a). Although Fig. 7(d) shows that the $R_{\Delta\lambda}$ increases with the current increasing, the increase in $R_{\Delta\lambda}$ is very small for the EDCC DFB laser. That is to say, as the current increases, the main mode moves towards the center, then slightly deviate from the center to the right side mode of the stopband. If the LSHB is not reduced, the deviation from the center is large with the current increasing, and the one side mode increases in intensity, while the other side mode retains a constant intensity, (i.e., the intensity difference will gradually increase) [18], [19]. However, for the EDCC DFB laser, the difference between the intensity of the left and right side modes are calculated based on the measured data is plotted in Fig. 7(b)(e). The result shows that the intensity difference between the two side modes decreases rather than increases with the injection current increasing, which is consistent with the variation in the SMSRs of the two side mode along with the injection current shown in Fig. 7(b). Based on the above analysis, the LSHB effect is effectively reduced in the EDCC DFB laser.

The lasing spectrums at the same injection current of 120 mA when the temperature is 25 °C, 35 °C, 45 °C, and 55 °C, respectively, are measured, the good SLM operation can be seen in Fig. 8(a). The corresponding $SMSR_L$ and $SMSR_R$ of the spectrum are plotted in Fig. 8(b). The tested results show that the minimal SMSR is 54.6 dB and the maximum SMSR is 56.1 dB, and the difference between the $SMSR_L$ and $SMSR_R$ is small. Although the $R_{\Delta\lambda}$ is a little larger

than 0.5, as shown in Fig. 8(b), i.e., the main mode slightly deviate from the center to the right side mode, Fig. 8(d) shows that the intensity difference between the two side modes is small. The calculated results based on the measured data shows that the maximum intensity difference between the two side modes is only 1.54 dBm, which is consistent with the results of the SMSRs of the two side mode in Fig. 8(b). Therefore, the LSHB is effectively reduced in the EDCC DFB laser, even at high temperature and large injection current.

5. Conclusion

The DCC DFB semiconductor laser is proposed, designed, and experimentally demonstrated by using the equivalent method. The phase-shift and DCC grating profile are equivalently realized by changing the sampling parameters while the seed grating is kept uniform. The EDCC DFB lasers always operate with the stable SLM, even at large injection current and high temperature. Stable SLM operation DFB laser is novelly developed by introducing discrete coupling coefficient structure.

References

[1] J. E. A. Whiteaway *et al.,* "The static and dynamic characteristics of single and multiple phase-shifted DFB laser structures," *IEEE J. Quantum Electron.*, vol. 28, no. 5, pp. 1272–1293, May 1992.
[2] Y. Yoshikuni and G. Motosugi, "Multielectrode distributed feedback laser for pure frequency modulation and chirping suppressed amplitude modulation," *J. Lightw. Technol.*, vol. LT-5, no. 4, pp. 516–522, Apr. 1987.
[3] M. Okai *et al.,* "Corrugation-pitch-modulated phase-shifted DFB laser," *IEEE Photon. Technol. Lett.*, vol. 1, no. 8, pp. 200–201, Aug. 1989.
[4] T. Fessant, "Enhanced dynamics of QWS-DFB lasers by longitudinal variation of their coupling coefficient," *IEEE Photon. Technol. Lett.*, vol. 5, no. 8, pp. 1075–1077, Aug. 1997.
[5] H. Zhu *et al.,* "The fabrication of eight-channel DFB laser array using sampled gratings," *IEEE Photon. Technol. Lett.*, vol. 22, no. 5, pp. 353–355, Mar. 2010.
[6] J. Zhao *et al.,* "Experimental demonstration of a 16-channel DFB laser array based on nanoimprint technology," *Semicond. Sci. Technol.*, vol. 28, no. 5, pp. 1–6, May 2013.
[7] S. Bao *et al.,* "Sampled grating DFB laser array by periodic injection blocking," *IEEE J. Sel. Topic Quantum Electron.*, vol. 19, no. 5, Feb. 2013, Art. ID. 1503008.
[8] J. Li *et al.,* "Experimental demonstration of distributed feedback semiconductor lasers based on reconstruction-equivalent-chirp technology," *Opt. Exp.*, vol. 17, no. 7, pp. 5240–5245, Mar. 2009.
[9] Y. Shi *et al.,* "A novel concavely apodized DFB semiconductor laser using common holographic exposure," *Opt. Exp.*, vol. 21, no. 13, pp. 16 022–16 028, Jul. 2013.
[10] S. Li *et al.,* "Experimental demonstration of DFB semiconductor lasers with varying longitudinal parameters," *Opt. Exp.*, vol. 22, no. 4, pp. 4059–4064, Feb. 2014.
[11] Y. Shi *et al.,* "High channel count and high precision channel spacing multi-wavelength laser array for future PICs," *Sci. Rep.*, vol. 4, p. 7377, Dec. 2014.
[12] Y. Shi *et al.,* "Study of the multiwavelength DFB semiconductor laser array based on the reconstruction-equivalent-chirp technique," *J. Lightw. Technol.*, vol. 31, no. 20, pp. 3243–3250, Oct. 2013.
[13] W. Li, X. Zhang, and J. Yao, "Experimental demonstration of a multi-wavelength distributed feedback semiconductor laser array with an equivalent chirped grating profile based on the equivalent chirp technology," *Opt. Exp.*, vol. 21, no. 17, pp. 19 966–19 971, Aug. 2013.
[14] Y. Zhang *et al.,* "Study on DFB semiconductor laser array integrated with grating reflector based on reconstruction-equivalent-chirp technique," *Opt. Exp.*, vol. 23, no. 3, pp. 2889–2894, Jan. 2015.
[15] L. Li *et al.,* "Phase-shifted distributed feedback laser with linearly chirped grating fabricated by reconstruction equivalent chirp technique," *Opt. Laser Tech.*, vol. 61, pp. 57–61, Sep. 2014.
[16] J. Zheng *et al.,* "An equivalent-asymmetric coupling coefficient DFB laser with high output efficiency and stable single longitudinal mode operation," *IEEE Photon. J.*, vol. 6, no. 6, Dec. 2014, Art. ID. 1502809.
[17] J. Li *et al.,* "Monolithic buried heterostructure DFB laser array for integrated optical interconnects and WDM systems," presented at Opt. Fiber Commun. Conf., San Francisco, CA, USA, Mar. 9–13, 2014, Paper Th3A.6.
[18] K. Utaka, S. Akiba, K. Sakai, and Y. Matsushima, "$\lambda/4$-shifted InGaAsP/InP DFB lasers," *IEEE J. Quantum Electron.*, vol. QE-22, no. 7, pp. 1042–1051, Jul. 1986.
[19] P. Correc, "Stability of phase-shifted DFB lasers against hole burning," *IEEE J. Quantum Electron.*, vol. 30, no. 11, pp. 2467–2476, Nov. 1994.